



## Research Paper

Preparation and Characterization of PIM-1/Modified Zeolite Mixed Matrix Membranes for CO<sub>2</sub>/N<sub>2</sub> separationSedra Tul Muntha<sup>1</sup>, Nusrat Shaheen<sup>1</sup>, Muhammad Siddiq<sup>2,\*</sup>, Asma Khan<sup>1</sup>, Tanzeela Fazal<sup>1</sup><sup>1</sup> Department of Chemistry, Abbottabad University of Science and Technology, Abbottabad, 22010, Pakistan<sup>2</sup> Department of Chemistry, Quaid i Azam University, Islamabad, 45320, Pakistan

## Article info

Received 2020-03-26

Revised 2020-05-05

Accepted 2020-05-05

Available online 2020-05-05

## Keywords

PIM-1

Gas separation

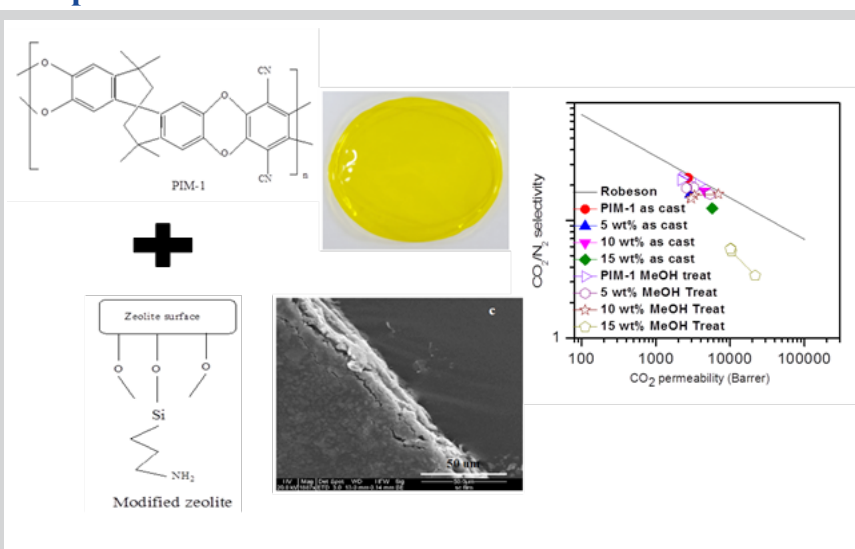
Modified zeolite

Methanol treatment

## Highlights

- TGA showed membranes are thermally stable up to 460°C.
- BET analysis of PIM-1 showed surface area of 656 m<sup>2</sup>g<sup>-1</sup> and 346 m<sup>2</sup>g<sup>-1</sup> for MZ.
- Incorporation of MZ significantly enhances the CO<sub>2</sub> permeability as compared to PIM-1 alone.
- The methanol treated membranes exhibit considerable increase in permeability.
- Membrane's performance with regards to CO<sub>2</sub>/N<sub>2</sub> selectivity is improved up to 10 wt% MMM.

## Graphical abstract



## Abstract

Mixed matrix membranes (MMMs) of polymer of intrinsic microporosity (PIM-1) is synthesized by incorporating modified zeolite (MZ) as the filler. Zeolite was treated with (3-Aminopropyl)-triethoxysilane (APTES). This treatment provided terminal amino groups to the zeolite by interaction between zeolite and ethoxy group of silane. MZ was systematically incorporated from 5 wt% to 15 wt% for evaluation of the improvement in gas separation behaviour. Physical characteristics and elemental analysis of MMMs were evaluated by X-ray photoelectron spectroscopy (XPS), X-ray diffraction analysis (XRD) and Fourier transform infrared (FTIR) spectroscopy. FTIR spectrum indicated physical interaction between PIM-1 and MZ. Scanning electron microscopy analysis (SEM) revealed the smooth surface morphology for PIM-1 membrane. Aggregates of MZ were observed from SEM analysis of PIM-1/MZ MMMs which indicated the formation of additional void volume. The Brunauer, Emmett, Teller (BET) analysis exhibited type I isotherm for PIM-1. The PIM-1 surface area was calculated to be 656 m<sup>2</sup>g<sup>-1</sup>. Thermogravimetric analysis (TGA) revealed that membranes are thermally stable up to 460°C. Gas separation behaviour of MMMs was also evaluated with particular focus on CO<sub>2</sub>/N<sub>2</sub> separation. Permeability was observed to increase with increasing filler concentration. CO<sub>2</sub> permeability was evaluated to increase from 2610 barrer for PIM-1 membrane to 5540 barrer for PIM-1/MZ MMM (15 wt%). Tremendous increase in permeability was observed for alcohol treated PIM-1/MZ MMMs. Aging analysis was performed by calculating the permeability for each membrane after 30, 60 and 90 days.

© 2021 MPRL. All rights reserved.

## 1. Introduction

Global warming is the world's critical environmental issue. Recent data reported that carbon dioxide (CO<sub>2</sub>) concentration in the environment has

reached 394 ppm which exceeds the safety limit of 350 ppm. Experts predicted that the current energy demands could increase the CO<sub>2</sub>

\* Corresponding author: E-mail address: m\_sidiq12@yahoo.com (M. Siddiq)

concentration to 570 ppm by the year 2100 [1]. Huge volume of flue gas should be treated for reduction of direct release of CO<sub>2</sub> to atmosphere.

CO<sub>2</sub> can be separated from flue gases through polymer gas separation membranes [2]. The pressure and concentration conditions strongly influence the performance of polymer membrane [3]. For gas separation membranes, bouquet of advantages are offered by polymers; great selectivity can be achieved by tailoring their chemistry, membranes can be thin, light and flexible due to ease of handling capability. Polysulfones, polycarbonates and polyimides are highly selective polymers but their permeability is low because they do not have adequate free volume.

PIMs have been extensively analysed for gas separation. Chain rigidity and high free volume of PIMs improves the membrane separation properties [4]. The contorted structure of PIMs distinguishes them from conventional polymers. However, decrease in permeability is exhibited by such polymers due to structural collapse over time [5]. The addition of porous material, a secondary phase, can reduce the aging process [6]. Addition of zeolite in PIMs is auspicious approach to surpass the upper bound by virtue of their enhanced separation capabilities. These MMMs can surpass the performance of unfilled polymer. Mason et al., prepared silicalite-1 reinforced PIM-1 MMMs [7]. Reinforcement of silicalite-1 crystals in PIM-1 matrix significantly improved gas permeation results. Improved selectivity of these membranes with reduced permeability located them above 2008 Robeson's upper bound. Khdayyer et al., synthesized MMMs by incorporating MIL-101 metal organic framework in PIM-1 matrix [8]. The membranes exhibited excellent combination of selectivity and permeability. The permeability ( $P_{CO_2}$ ) of 35,600 Barrer was achieved. Alentiev et al., reported gas permeation properties of MIL-101 reinforced PIM-1 MMMs [9]. The diffusion coefficient and permeability of MMMs was enhanced for (N<sub>2</sub>, He, CO<sub>2</sub>, O<sub>2</sub>) gases.  $P_{CO_2}$  was increased from 3250 Barrer to 8440 Barrer with increasing filler concentration. Khdayyer et al. synthesized PIM-1/UiO-66 MOF MMMs for CO<sub>2</sub>/CH<sub>4</sub> separation [10]. With increasing concentration of filler, permeability was increased. Selectivity was observed to maintain for amine modified UiO-66. Ye et al., reported the effect of ZIF-67 loading on selectivity of PIM-1 [11]. About 69.40% enhancement was observed for CO<sub>2</sub>/CH<sub>4</sub> selectivity. Enhanced selectivity was ascribed to improved interfacial interactions of filler-polymer.

Zeolite is well-known inorganic material constituting microporous structure having SiO<sub>4</sub> and AlO<sub>4</sub> (aluminosilicate) tetrahedral [12]. While fabricating MMMs for separation applications, molecular sieving phase must give definite shape and size distinction [13]. Porous zeolites attract increased attention over non-porous fillers due to their characteristic capacity to act as a secondary transport pathway when added to polymer matrix. Junaidi et al., synthesized polysulfone/SAPO-34 zeolite MMM by phase inversion method to investigate CO<sub>2</sub>/N<sub>2</sub> separation properties [14]. The 10 wt% polysulfone/zeolite MMM showed enhanced CO<sub>2</sub>/N<sub>2</sub> separation performance as compared to neat polysulfone membrane. On higher zeolite loading, the permeation properties were observed to disrupt because particle agglomeration results in formation of large interfacial voids. Chaidou et al., synthesized polyimide/zeolite MMMs for gas separation analysis [15]. He observed an increase in permeability with increase in zeolite loading. Kausar et al., fabricated polycarbonate/poly(styrene-co-allyl alcohol)/nano-zeolite MMMs for CO<sub>2</sub>/N<sub>2</sub> separation [16]. CO<sub>2</sub> permeability of 114.5 Barrer was observed. Optimal results were exhibited by 10 wt % MMM which showed improved selectivity of 38.2.

Selectivity ( $\alpha(A/B)$ ) and permeability co-efficient ( $PA$ ) are the fundamental parameters which characterize the separation performance of membrane [17]. To make the polymer desirable for separation performance, it should have high selectivity and permeability. Higher purity is resulted from higher selectivity. High permeable membrane requires less area to treat the gas, thus, decreases the membrane's capital cost. However, more permeable polymers are less selective. This trade off relationship is quantified by Robeson et al. [18]. He used double logarithmic plot of selectivity vs, permeability. The most implicit membranes are described by the line 'upper bound' on plot.

Althumayri et al., fabricated PIM-1/graphene MMMs for investigation of gas separation properties [19]. Significant enhancement was observed in permeability of MMMs at low graphene concentration. The permeability for CO<sub>2</sub> was substantial even after eight months as compared to unfilled polymer. Mitra et al., prepared PIM-1/hyper crosslinked polystyrene MMMs for CO<sub>2</sub>/N<sub>2</sub> separation [20]. The CO<sub>2</sub> permeability was observed to increase from 2,660 barrer for PIM-1 membrane to 10,040 barrer for PIM-1/hyper crosslinked polystyrene MMM (17 wt%). Bushell et al. prepared PIM-1/ZIF-8 MMMs for investigation of permeation properties [21]. Permeability was observed to be enhanced by ethanol treatment. Free volume is increased by combination effect of loosely packed polymer chains and the contribution cavities at interface between ZIF-8 and PIM-1.

In this work we report fabrication of PIM-1/MZ MMMs with synergic separation performance. The fundamental understanding of science and

engineering for PIM-1/MZ MMMs fabrication are provided. The zeolite particles were modified through silane treatment to reduce the polymer-particle interfacial defects. The modified zeolite particles were reinforced to PIM-1 matrix at varying concentrations (5 wt%, 10 wt%, 15 wt%). Single gas permeation data was calculated for as cast and methanol treated MMMs. Aging analysis was performed on methanol treated MMMs after 30 days, 60 days and 90 days. Permeability coefficients ( $P$ ) and selectivity for the gas pair CO<sub>2</sub>/N<sub>2</sub> were calculated at ambient temperature (298K). The trade-off between selectivity and permeability as well as physical aging of polymers requires a search for new synthesis routes to control and improve polymer architecture.

## 2. Experimental

### 2.1. Materials

5,5',6,6'-tetrahydroxy-3,3,3',3'-tetramethyl-1,1'-spirobisindane (TTSBI, 98%) was procured by Alfa Aesar. Dicyanotetrafluorobenzene (98%) was purchased from Aldrich. Dicyanotetrafluorobenzene was dissolved in acetone and washed with distilled water before use. Potassium carbonate (K<sub>2</sub>CO<sub>3</sub>, 99%) was supplied by Fisher. K<sub>2</sub>CO<sub>3</sub> was dried for 24 hours in vacuum oven at 110 °C before use. Zeolite A-3 granular with average size of 7µm were supplied by Daejung. (3-aminopropyl)-trimethoxysilan (APTMS, 99%), dimethyl acetamide (DMAc, 99.8%), chloroform (99.9%) and toluene (99.7%) were purchased from Aldrich and were used as such. Carbon dioxide (CO<sub>2</sub>) and nitrogen (N<sub>2</sub>) of purity 99.995% and 99.999% were supplied by BOC Gases and were used as received.

### 2.2. Instrumentation

Gel permeation chromatography, GPC, (Viscotek 2001) was used for investigation of molecular weight ( $M_w$ ) by using 2 mixed B 500 A<sup>+</sup> polymer laboratories PL gel columns. Thermo Scientific™ Nicolet iS5 FT-IR Spectrometer with an attenuated total reflectance (ATR) accessory was used to record infra-red spectra (IR) of samples. X-ray photoelectron spectroscopy (XPS) was determined by using a Kratos Axis Ultra DLD spectrometer with a monochromated Al K-alpha X-ray source (E = 1486.6 eV, 10 mA emission). Elemental analysis was performed by using a Thermo Scientific Flash 2000 organic elemental analyser (CHNS analyser). Thermogravimetric analysis (TGA) was performed using a Mettler Toledo star system. The samples were heated to 1000 °C at the rate of 10 °C/min under inert atmosphere. Micromeritics ASAP 2020 porosity and surface area analyser was used to calculate Brunauer-Emmet-Teller (BET) surface area from N<sub>2</sub> adsorption isotherms. Membrane morphology was studied by Scanning electron microscopy (SEM) by using a Hitachi S-4800 field-emission scanning electron microscope. Samples were coated with gold by sputtering through Emitech coater before analysis. X-ray diffraction patterns (XRD) were recorded using a Philips high X'pert pro diffraction system model PW3040/60 and X'Pert data collector version 2.0d software, with Cu Kα X-ray radiation. Standard variable volume method was carried out for permeability measurement using pure gases (CO<sub>2</sub> and N<sub>2</sub>) at 2 atm upstream gas pressure and ambient temperature of 298K.

### 2.3. Synthesis of PIM-1

Budd et al. [22] method was followed for synthesis of PIM-1. The chemical reaction for synthesis of PIM-1 is shown in Scheme 1. TTSBI (0.05 mol), dicyanotetrafluorobenzene (0.05 mol) and K<sub>2</sub>CO<sub>3</sub> (0.15 mol) were added to dry round bottom flask (500 mL) equipped with condenser and mechanical stirrer. Toluene (50 mL) and DMAc (100 mL) were poured to above mixture under nitrogen environment. Mixture was set to reflux for 40 min at 160 °C. The reaction product was precipitated to methanol (500 mL) and then dissolved in chloroform (500 mL). The product was refluxed in deionised water for 15 hours. The final product was washed with acetone and dried. The yield of PIM-1 was 19.89gm (81% yield). The gel permeation chromatogram of PIM-1 is shown in Figure 1. The absolute weight average molar mass ( $M_w$ ) for PIM-1 is determined as 131,968 g/mol, number average molar mass ( $M_n$ ) is determined as 37,721 g/mol, polydispersity index (PDI) is calculated as 3.49. The synthesized polymers are characterised by high molecular weight. Satilmis et al., reported PIM-1 of  $M_w$  100,000 [23]. Anal. Calc. for C<sub>29</sub>H<sub>20</sub>N<sub>2</sub>O<sub>4</sub> (wt%) : C, 75.64; N, 6.08; H, 4.37 Found: C, 74.36; N, 6.01; H, 4.38.

### 2.4. Zeolite modification

Modification of zeolite has been discussed in detail in our previous

publication [24]. Mixture of zeolite in 1,1,1-trichloroethane was prepared. APTMS was dropwise added and mixture was set to reflux at 60 °C. This treatment provided terminal amino groups to zeolite.

### 2.5. Synthesis of PIM-1 membrane

PIM-1 (0.3 g) was dissolved in anhydrous chloroform ( $\text{CHCl}_3$ , 10mL) and mixture was set to overnight stirring to ensure the homogeneity of casting solution. Glass wool was used to filter casting solution. It was placed in a closed environment for 48 hours. Membrane was formed by slow solvent evaporation process.

### 2.6. Synthesis of PIM-1/MZ mixed matrix membranes

MMMs of PIM-1 with MZ were prepared in  $\text{CHCl}_3$  in three different proportions (5 wt%, 10 wt%, 15 wt% of MZ particles). The interaction between PIM-1 and MZ is represented in Scheme 2. Weight % of filler in mixed matrix membranes was calculated by following formula [20]:

$$\text{wt\% of filler in MMMs} = 100 \times \frac{\text{wt of filler}}{\text{wt of filler} + \text{wt of PIM-1}} \quad (1)$$

For preparation of PIM-1/MZ MMM, a suspension of MZ was prepared in  $\text{CHCl}_3$ . At ambient temperature, it was stirred for 12 hours. This was followed by sonication. A chloroform solution of PIM-1 was poured to the suspension. Mixture was set to stir for 20 hours. This was followed by sonication in an ultrasonic bath type sonicator for 20 minutes. Resulting solution was placed in a closed nitrogen environment for 48 hours where membrane was formed by slow solvent evaporation process. The fabricated membranes were kept under vacuum in a desiccator until used for characterization.

### 2.7. Methanol treatment of mixed matrix membranes

The casting conditions (e.g., selection of solvent) may affect the gas permeation performance of PIM-1 membrane. However, alcohol can be used as a useful source for comparing different membranes due to its properties of washing away the leftover casting solvent and hence opens up the structure of PIM-1. Thus permeability can be increased on high scale by using alcohol. [25]. For this purpose, membranes were soaked overnight in methanol. The methanol treated membranes were kept under vacuum in desiccator for 1 h before gas permeation studies.

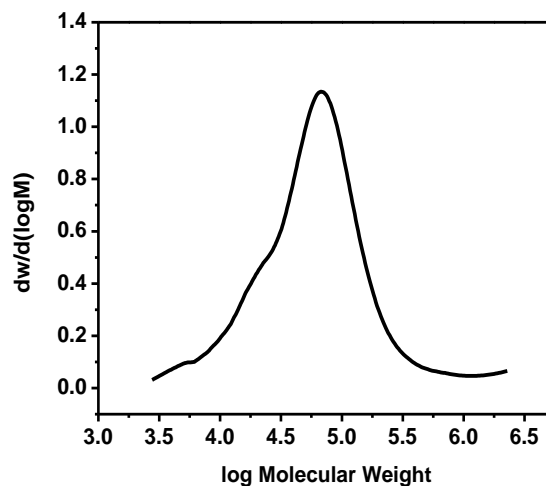
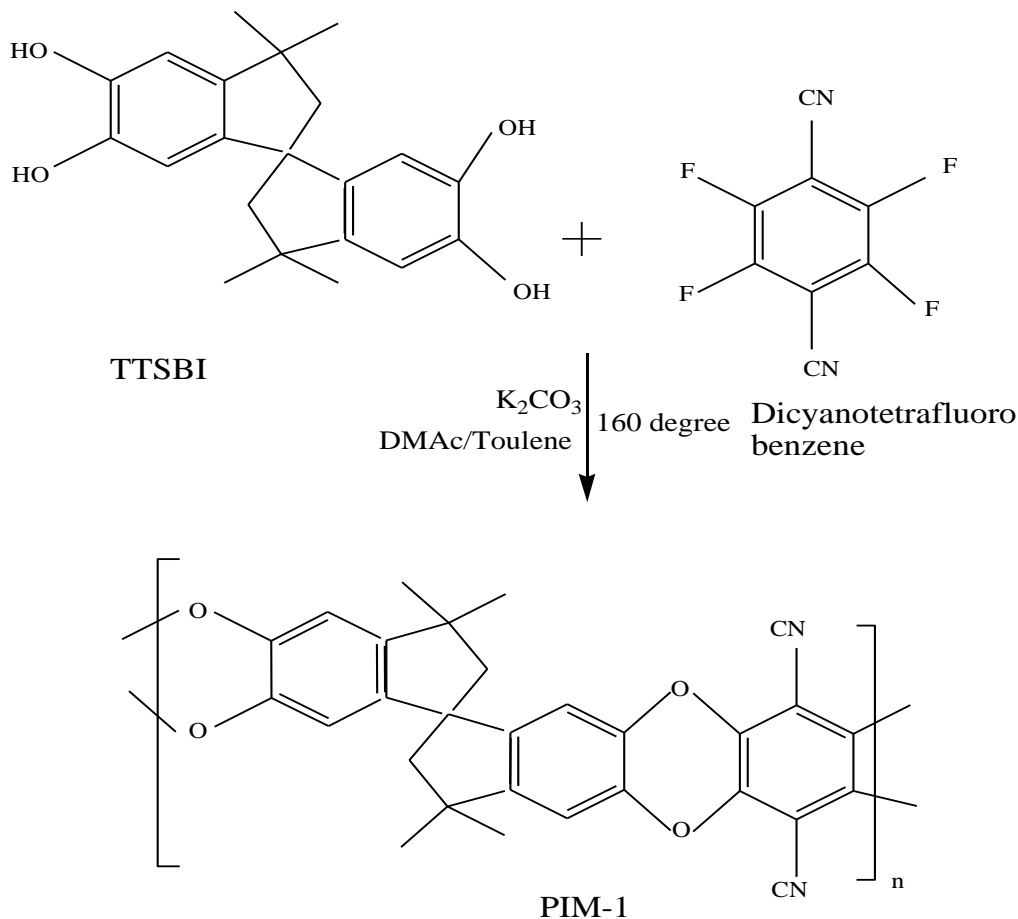


Fig. 1. GPC curve of PIM-1.



Scheme 1. Synthesis of PIM-1.

### 2.8. Single gas permeation measurements

Gas permeation analysis of single gases was performed at 298K using the standard variable volume method [20,26]. Membranes were evacuated carefully for removal of any dissolved specie. The  $N_2$  was tested first and then  $CO_2$  was tested.  $2.4 \text{ cm}^2$  membrane's area was used. In permeate volume, pressure increase was monitored by pressure transducer. Gas permeability was calculated by following formula [20].

$$P = \frac{N \cdot l}{P_1 - P_2} \quad (2)$$

$P$  is permeability co-efficient (Barrer),  $l$  is thickness of the membrane (cm),  $P_1$  is the feed side pressure and  $P_2$  is the permeate side pressure,  $N$  is the steady state penetrant flux ( $\text{cm}^3\text{cm}^{-2}\text{sec}^{-1}$ ). For a pair of gases,  $A$  and  $B$ , ideal selectivity is the ratio of permeabilities [27],

$$\alpha_{A/B} = \frac{P_A}{P_B} \quad (3)$$

For each membrane, ten thickness measurements were made using a digital micrometre (Mitutoyo).

## 3. Results and discussion

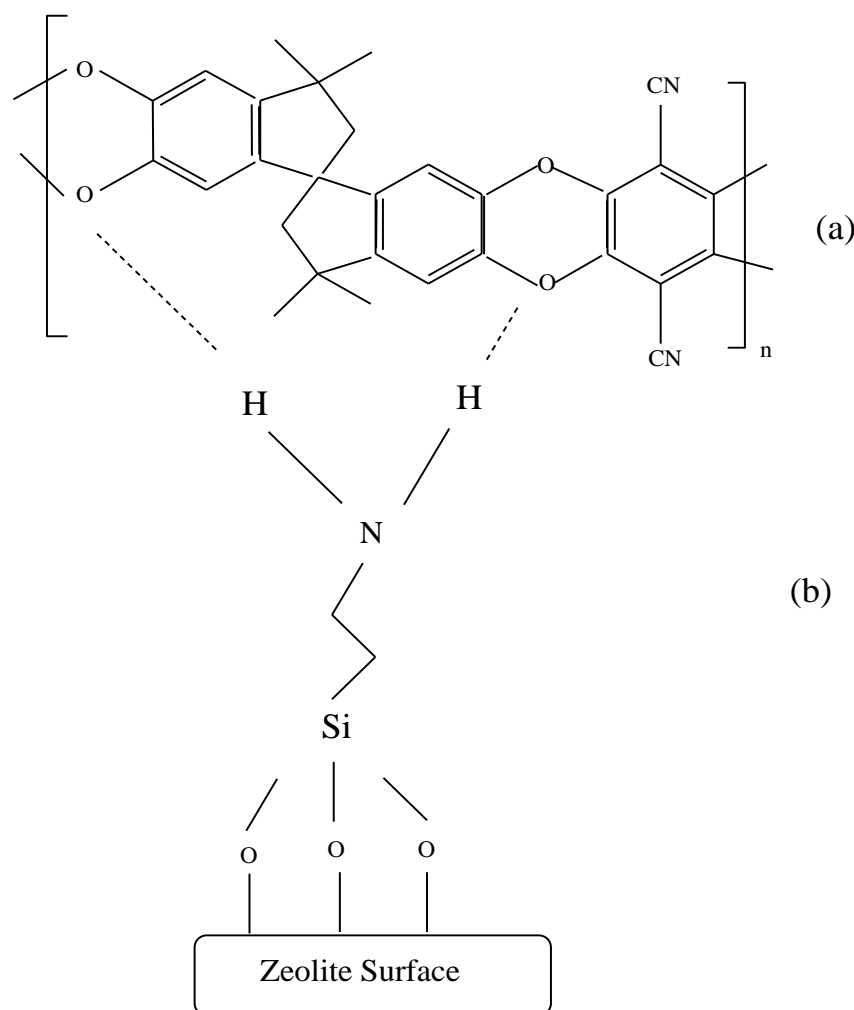
### 3.1. Spectroscopic analysis

ATR-IR spectroscopy is performed to identify the functional groups. The spectrum of MZ is depicted in Figure 2a. Al-O symmetric stretching vibration

gives signal intensity at  $1024 \text{ cm}^{-1}$ . The absorption at  $1526 \text{ cm}^{-1}$  is ascribed to N-H bending. Si-H bond gives sharp peak at  $2346 \text{ cm}^{-1}$ . Absorption at  $3597 \text{ cm}^{-1}$  is attributed to residual OH groups. From the ATR-IR spectra of PIM-1 membrane (Figure 2b), the characteristic peak at  $2236 \text{ cm}^{-1}$  is associated to  $-C\equiv N$  symmetric stretching. Physical interaction is predicted between PIM-1 and modified zeolite as the peak intensities are observed to decrease for  $-C\equiv N$  and C-O group in PIM-1/MZ MMM (Figure 2c) which indicates the presence of hydrogen bonding. Distinct peak at  $2952 \text{ cm}^{-1}$  is ascribed to C-H symmetric stretching vibration. The characteristic absorptions at  $1450 \text{ cm}^{-1}$  and  $1015 \text{ cm}^{-1}$  corresponds to C=C and C-O symmetric stretching vibration. Weak IR reflections generated weak IR signals due to dark colour of PIM-1 membrane [28].

### 3.2. XPS analysis

To investigate the elemental composition of fabricated samples, XPS analysis is performed. In Figure 3a, XPS survey scan of fabricated PIM-1 membrane is reported. The peak at  $281.6\text{eV}$  is associated to C 1s while the peak at  $529.41\text{eV}$  is attributed to O 1s. The prominent peak at  $397.26\text{eV}$  is ascribed to nitrile group in the PIM-1 structure. The Figure 3b depicts the XPS survey scan of MZ particles. The peaks for elements O, N, Si and Al can be identified. The binding energy  $396.2\text{eV}$  is assigned to N 1s. The signal at  $531\text{eV}$  confirms the presence of O 1s. The peak at  $99 \text{ eV}$  corresponds to Si 2p. Minor Al 2p is also detected in the XPS spectra of MZ. The XPS survey scan of PIM-1/MZ MMM is represented in Figure 3c. The spectrum confirms the presence of C, O, Si and Al. The presence of  $C\equiv N$  is confirmed with a binding energy of  $395.4 \text{ eV}$ .



Scheme 2. Interactions between (a) PIM-1 and (b) MZ.

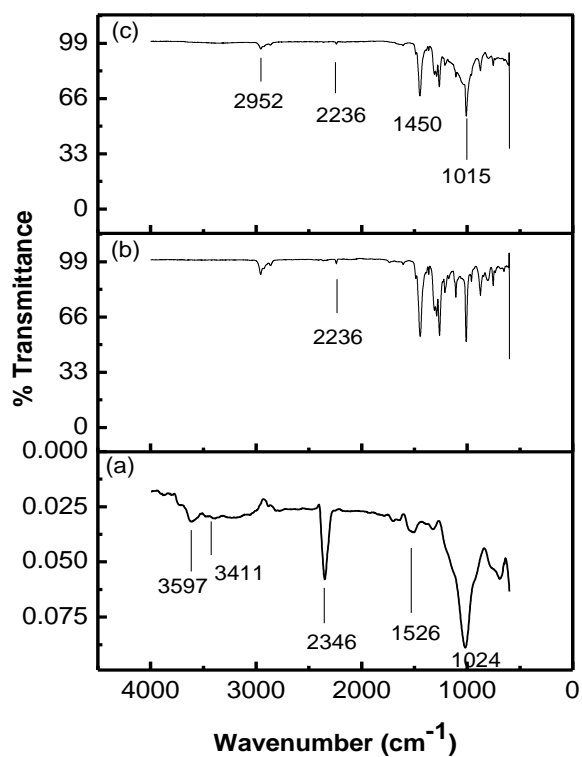


Fig. 2. ATR-IR spectrum of (a) MZ; (b) PIM-1 membrane; (c) PIM-1/MZ MMM (15 wt%).

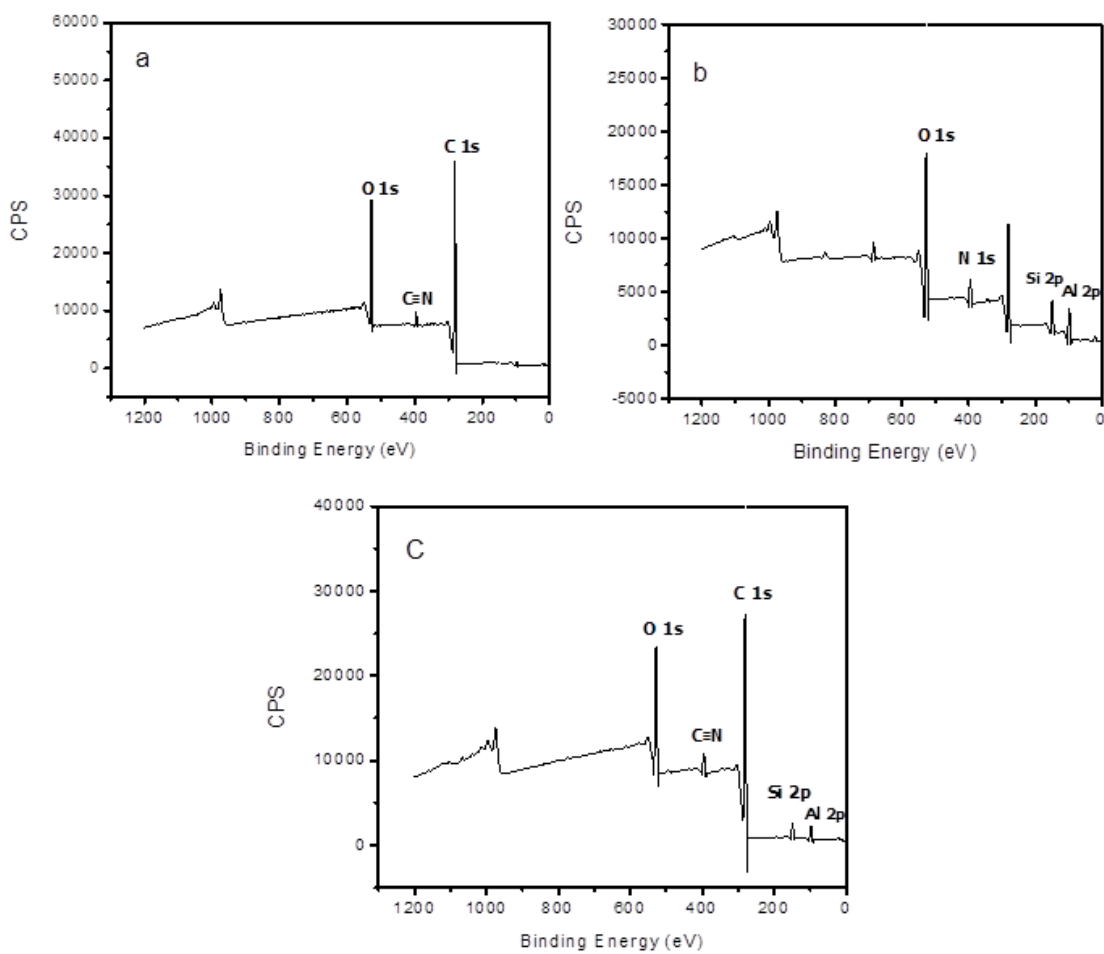


Fig. 3. XPS survey scan of (a) PIM-1 membrane; (b) MZ; (c) PIM-1/MZ MMM (15 wt%).

### 3.3. Morphological investigation

Details about surface and morphology of synthesized mixed matrix membranes are examined through SEM analysis. SEM analysis of surface of PIM-1 membrane, PIM-1/MZ MMM and MZ particles are depicted in Figure 4. For PIM-1 membrane, smooth morphology and homogenous phase is observed (Figure 4a). SEM micrograph of MZ exhibit brittle fractured surface (Figure 4b). The MZ particles tend to agglomerate showing low dispersibility. Tubular morphology which is an indication of clinoptilolite is observed [24]. The SEM image of PIM-1/MZ MMM at 15wt% MZ loading is shown in Figure 4c. The MZ particles are not distributed well all through PIM-1 matrix and tends to agglomerate. Also the interface voids and defects are detected around the surface of MMM. Inter-aggregate spacing can be seen between aggregates which results in generation of additional void volume. Usually preparation of zeolite filled PIM-1 membrane results in interface voids due to adherence issues between inorganic and organic phases. In specific the interface morphology of polymer/inorganic filler is crucial of overall transport properties.

### 3.4. BET surface area analysis

Free volume of PIM-1 is analysed through low pressure gas sorption ( $N_2$ ) at  $-196^\circ C$ . The low pressure  $N_2$  sorption isotherm of PIM-1 is shown in Figure 5a. PIM-1 shows type I isotherm which is an indication of significant microporosity. Hysteresis is observed on desorption. It can be attributed to pores network effect. The microporosity of PIM-1 is attributed to its high rigidity in combination with contorted shape. It arises wholly from molecular structure. Therefore, it is termed as intrinsic. The nitrogen adsorption-desorption isotherm of MZ was calculated at  $-196^\circ C$ . The low pressure  $N_2$  sorption isotherm for MZ is generally of type IV as depicted in Figure 5b. Zeolites are crystalline alumina-silicates. The BET analysis revealed capillary condensation and microporosity as adsorption hysteresis loop is observed at

higher  $P/P$  [29]. The surface area calculations of synthesized PIM-1 and MZ are reported in Table 1.

**Table 1**  
Pore volume and BET surface area.

Sample	Surface Area ( $m^2g^{-1}$ )	Pore Volume ( $cm^3g^{-1}$ )	Pore Size (nm)
PIM-1	656	0.24	2.1
MZ	346	0.207	2.6

### 3.5. Thermal analysis

The thermal stabilities of PIM-1 mixed matrix membranes are examined by TGA. Figure 6 depicts the degradation curves of PIM-1/MZ mixed matrix membranes. The membranes are thermally stable up to  $460^\circ C$ . The stability can be attributed to the dipolar interactions of nitrile groups. Nitrile group has strong dipole moment and high molecular association. Strong polarity arise from charge distribution between carbon and nitrogen atoms. The nitrogen atom of nitrile group has lone pair orbital along molecular axis. These factors impart strong polarity to nitrile group. Mixed matrix membranes display little weight loss due to mutual interaction of zeolite-amine of modified zeolite. Chatti et al., reported 22.56% weight loss for amine modified zeolite which was higher 4% as compared to unmodified zeolite [30]. Adsorbed moisture and volatile organics may be associated for weight loss below  $150^\circ C$ . The degradation temperatures of fabricated membranes are depicted in Table 2.

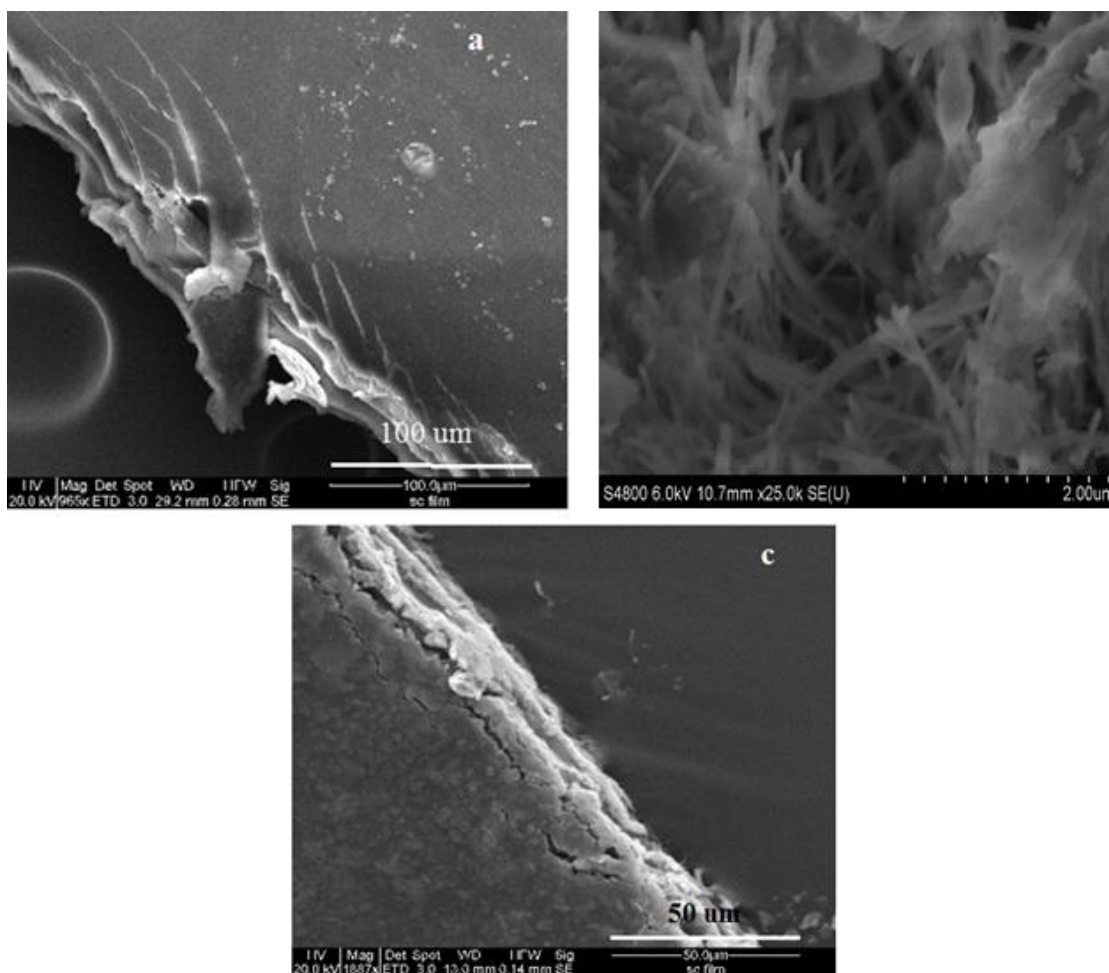


**Fig. 4.** SEM micrograph of membrane surface (magnification 20 kV) (a) PIM-1 membrane (100  $\mu m$ ); (b) MZ particles (2  $\mu m$ ); (c) PIM-1/MZ MMM (15 wt%) (50  $\mu m$ ).

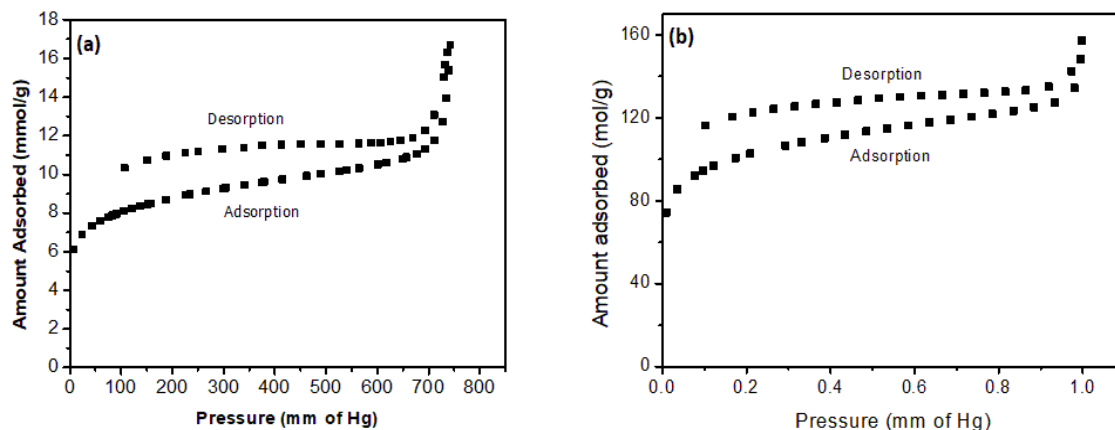


Fig. 5. (a) Low pressure N<sub>2</sub> sorption isotherm of PIM-1; (b) Low pressure N<sub>2</sub> sorption isotherm of MZ.

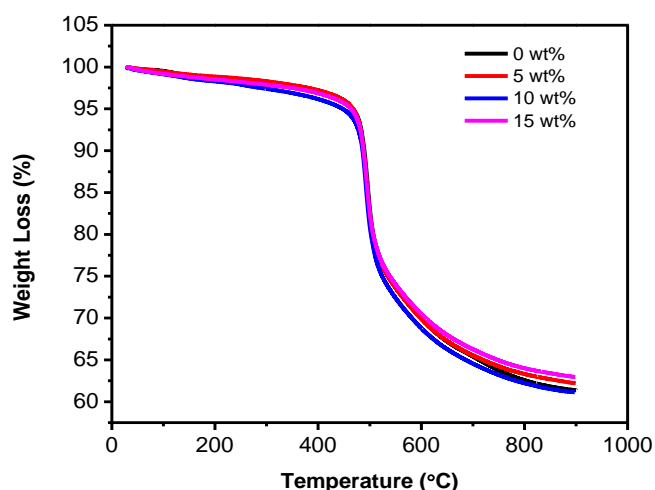


Fig. 6. TGA curves of PIM-1 membrane; PIM-1/MZ MMM (5wt%); PIM-1/MZ MMM (10 wt%); PIM-1/MZ MMM (15 wt%).

### 3.6. XRD analysis

PIM-1 is an amorphous glassy polymer. The XRD diffractogram of PIM-1 membrane is shown in Figure 7a which exhibit peaks with maxima at  $2\theta = 25.8^\circ$  and  $28.2^\circ$ . Tian et al., reported characteristic peak at  $22.6^\circ$  for PIM-1 with d-spacing of  $3.9 \text{ \AA}$  [31]. The diffraction peaks of MZ are observed at  $2\theta = 22.4^\circ$ ,  $25.8^\circ$  and  $27.8^\circ$  with the d-spacing of 3.9, 3.4 and  $3.2 \text{ \AA}$  (Figure 7b). Scherrer formula is used to calculate the average crystallite size of MZ particles which is 12 nm.

$$d = \frac{K\lambda}{B \cos\theta} \quad (4)$$

In equation (4),  $d$  is the average crystallite size,  $K$  is Scherrer constant,  $B$  is the FWHM of peak,  $\lambda$  is x-ray wavelength,  $\theta$  is Bragg angle [32]. The analysed nanocomposites do not have crystals of uniform size. The crystal size attained using this formula is 20% - 40% correct. Figure 7c shows the X-ray diffraction pattern of PIM-1/MZ MMM. Intensity of peaks is observed to increase due to presence of MZ particles in PIM-1 matrix. It is also an indication of interaction between PIM-1 and MZ particles. Bragg's equation is used to calculate the d-spacing of membranes.

$$n\lambda = 2d \sin\theta \quad (5)$$

where, wavelength of incident beam is  $\lambda$ , refractive index ' $n$ ' takes integer value in most cases,  $2\theta$  is the angle of diffraction between scattered and incident x-rays,  $d$  is the interlayer spacing of lattice planes. The calculations of d-spacing and degree of crystallinity (Xc) are summarised in Table 3. Xc is

calculated by dividing the area under crystalline region into the sum of area under amorphous and crystalline region [33].

Table 2  
Thermal analysis of PIM-1/MZ MMM.

Membrane	Td <sub>5%</sub> (°C)	Td <sub>max</sub> (°C)	Residual Mass (%)
PIM-1/MZ (0 wt%)	451	510	75.86
PIM-1/MZ (5 wt%)	456	516	76.54
PIM-1/MZ (10 wt%)	447	508	73.92
PIM-1/MZ (15 wt%)	458	518	77.12

Table 3  
d-spacing and crystallinity analysis of PIM-1 membrane, PIM-1/MZ MMM (15 wt%).

Membrane	2 $\theta$ position	d-spacing (Å)	Xc
PIM-1	25.8	3.45	41.39
PIM-1/MZ (15 Wt%)	28.1	3.18	47.26

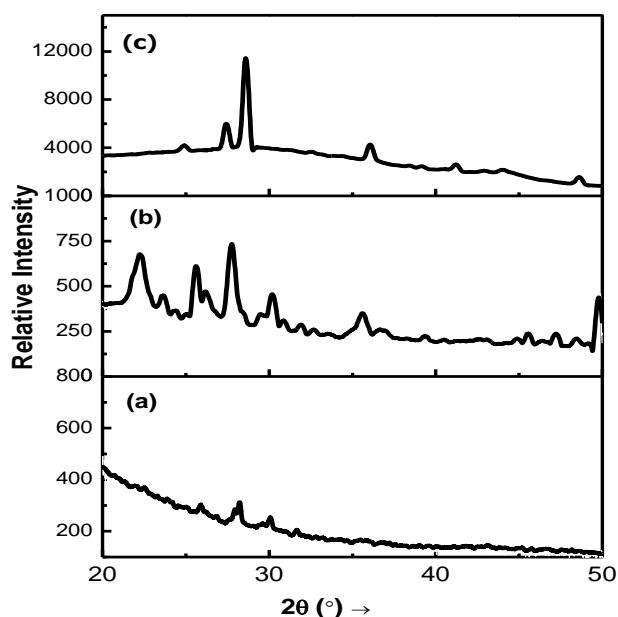


Fig. 7. XRD patterns of (a) PIM-1 membrane; (b) MZ; (c) PIM-1/MZ MMM (15wt%).

### 3.7. Gas separation analysis

The single gas permeation data of PIM-1/MZ MMMs are obtained and shown in Figure 8A. Permeability coefficients,  $P$ , are calculated for  $\text{CO}_2$  and  $\text{N}_2$  at ambient temperature (298K). The permeability of PIM-1 membrane is observed to increase with increasing filler content from 5 to 15 wt%. Similar result is observed by Bushell et al., for loading of ZIF-8 in PIM-1 [34]. Internal porosity of filler allow gas molecule to perforate more easily. Moreover, the nature of interface between filler-polymer, filler's effect on chain packing, thus the distribution of free volume in polymer are the parameters on which transport behaviour depends. Gas transport is directed through free volume regions in PIM-1. Over the time, relaxation in polymer chain reduces the free volume. However, reinforcement of inorganic filler improves the gas solubility and sieving properties of membrane. Polymer chain mobility is controlled by polymer-filler interfacial regions. For comparison, the membranes are treated with methanol. Considerable increase is observed in permeability of methanol treated MMM. This is because the residual solvent can be washed away by alcohol. Moreover, methanol treatment swells the membrane thus opens up the free volume [35]. However, an abrupt increase is observed in permeability of 15 wt% methanol treated MMM. The formation of undesirable channels and nonselective voids seems inevitable resulting in gas molecules bypassing the defects [36]. Selectivities of PIM-1/MZ MMM are determined for  $\text{CO}_2/\text{N}_2$  gas pair at ambient temperature (298K) and shown in Figure 8B. Significant drop is observed in selectivity of as cast PIM-1/MZ MMM on filler addition from 5 to 15 wt%. This is in accordance with Robeson observation that permeability is generally increased at cost of selectivity. In the selective layer, microvoids are present which arise from poor adherence with polymer matrix. High permeability pathways may be provided by microvoids but at cost of selectivity [28]. For methanol treated MMM, selectivity is observed to decrease with 5 wt% filler addition. However, from 5 to 10wt%, a little drop is observed in selectivity

regardless of increase in permeability over this range of filler. An abrupt decrease is observed in selectivity at higher filler concentration (15 wt%) for methanol treated membrane. This abrupt decrease may arise due to generation of nonselective voids and interfacial defects. A comparison of permselectivity values of as-cast and methanol treated MMMs are represented in Table 4.

For self-standing membranes, permeability may reduce over timescale. However, physical aging is accompanied often by increase in selectivity. Aged membranes impart positive changes for gas separation if the permeance of initial membrane is high enough. The gas transport properties for aging membranes are reported in Table 5. Upon aging of methanol treated PIM-1/MZ MMMs, faster loss of permeability is observed. Faster aging is shown by methanol treated membranes, losing up to 53%  $\text{CO}_2$  permeability after 90 days. The aging property of each membrane is summarized in Figure 9. Separation performance of aged PIM-1/MZ MMMs for  $\text{CO}_2/\text{N}_2$  is comparable to the reported values in literature. Mitra et al., reported the loss of  $\text{CO}_2$  permeability up to 50% after physical aging for PIM-1/HCP MMMs [17]. Alberto et al., reported the loss of  $\text{CO}_2$  permeability up to 62% after 155 days for PIM-1/graphene oxide MMMs [37]. In most cases, performance of fabricated MMMs is in accordance with the Robeson 2008 upper bound represented in Figure 10. Optimum performance is shown by methanol treated PIM-1/MZ MMM (10 wt%). Hence, the membrane's performance with regards to  $\text{CO}_2/\text{N}_2$  selectivity is improved up to 10 wt% MMM. Additionally, incorporation of MZ significantly enhances the permeability of  $\text{CO}_2$  as compared to PIM-1 alone. Comesaña-Gándara et al., redefined 2008 Robeson upper-bound for  $\text{CO}_2/\text{N}_2$  separation [38]. They reported gas permeability data of benzotriptycene based PIMs. All of the data was above 2008 upper-bound. Data points for  $\text{CO}_2$  permeability were distributed over large range of 4400 to 52,000 Barrer. The impressive performance resulted from high  $D\text{CO}_2/D\text{N}_2$  of 2.

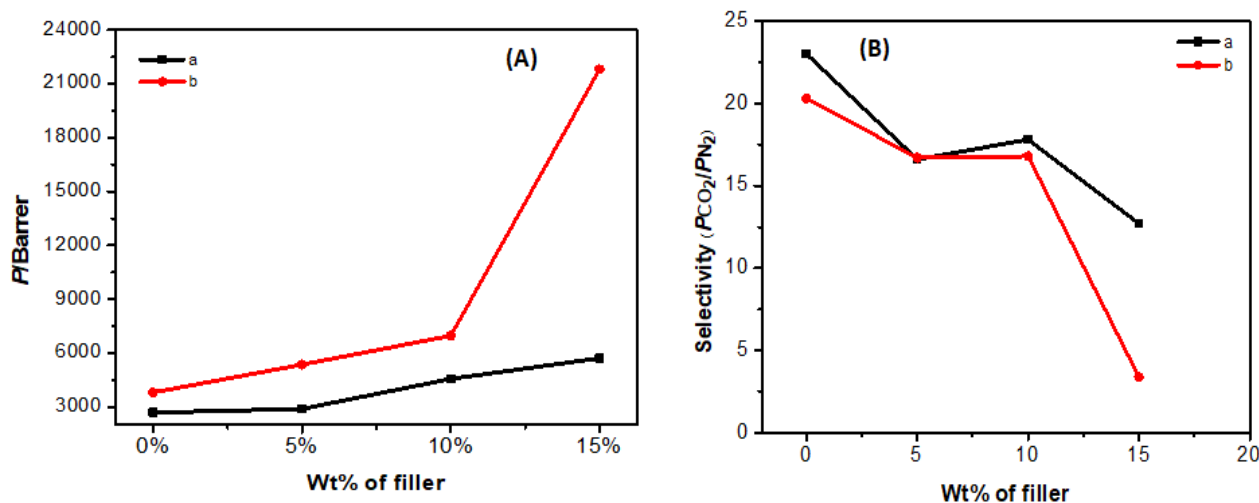


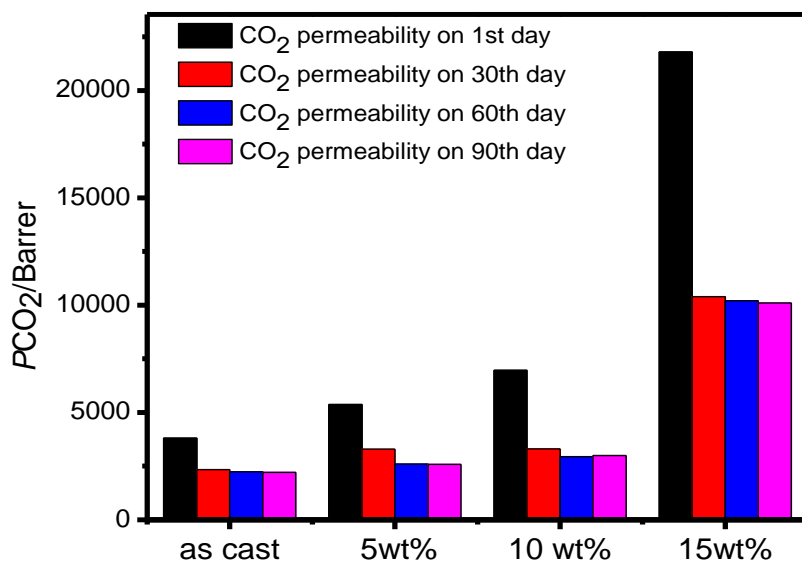
Fig. 8. (A) Dependence of permeability coefficient of  $\text{CO}_2$ . (a) As cast PIM-1/MZ MMM (b) Methanol treated PIM-1/MZ MMM; (B) Dependence of ideal selectivity relative to  $\text{N}_2$ . (a) As cast PIM-1/MZ MMM (b) Methanol treated PIM-1/MZ MMM. All data are shown for non-aged membranes.

Table 4  
Permeability coefficient in Barrer of as cast and methanol treated PIM-1/MZ MMMs

Wt. % of filler in PIM-1	As cast			Methanol Treated		
	$P(\text{CO}_2)$ (Barrer)	$P(\text{N}_2)$ (Barrer)	$\alpha(\text{CO}_2/\text{N}_2)$	$P(\text{CO}_2)$ (Barrer)	$P(\text{N}_2)$ (Barrer)	$\alpha(\text{CO}_2/\text{N}_2)$
0	2610	114	23	3690	185	20.3
5	2810	169	16.8	5200	311	16.7
10	4420	252	16.6	6570	390	16.8
15	5540	437	12.7	21100	6070	3.4

**Table 5**  
Ageing analysis of gas transport properties of PIM-1/MZ MMMs

Wt. % of filler in PIM-1	$P(\text{CO}_2)$ on 1 <sup>st</sup> day (Barrer)	$P(\text{CO}_2)$ on 30 <sup>th</sup> day (Barrer)	$P(\text{CO}_2)$ on 60 <sup>th</sup> day (Barrer)	$P(\text{CO}_2)$ on 90 <sup>th</sup> day (Barrer)
0	3810	2340	2230	2210
5	5370	3290	2600	2580
10	6970	3300	2940	3000
15	21800	10400	10200	10100



**Fig. 9.** Permeability and aging characteristics of PIM-1/MZ MMM.

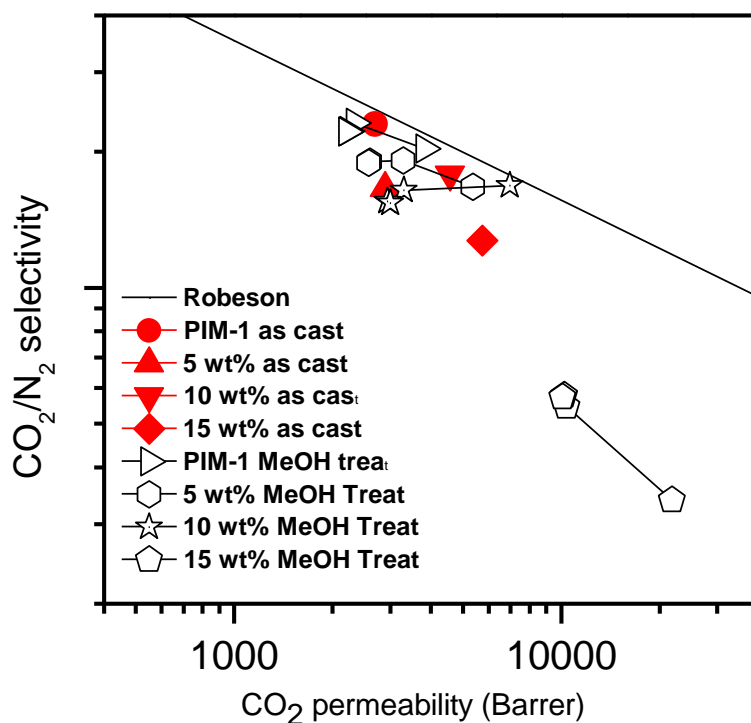


**Fig. 10.** The single gas CO<sub>2</sub> permeability and ideal CO<sub>2</sub>/N<sub>2</sub> selectivity of PIM-1 based MMMs plotted against Robeson 2008 upper bound. The filled shapes represent as-cast membranes while unfilled symbols represent analogous films after methanol treatment.

#### 4. Conclusions

Synthesis of MMMs by using PIM-1 and modified zeolite has been described. The reinforcement of modified zeolite in PIM-1 results in increasing permeability. The morphological investigations of MMMs revealed aggregation of MZ particles in PIM-1. This aggregation results in formation of inter-aggregate spacing which creates additional void volume. The surface area of  $656 \text{ m}^2\text{g}^{-1}$  and  $346 \text{ m}^2\text{g}^{-1}$  was calculated for PIM-1 and MZ. Therefore, the permeability is averaged over both polymer phase and filler phase. The thermal analysis of MMMs revealed good stability which can be attributed to the dipolar interactions of the nitrile group of PIM-1. The XRD analysis of PIM-1 revealed its amorphous nature. Interaction between PIM-1 and MZ is indicated from the XRD spectrum of PIM-1/MZ MMM (15 wt%), as the peak intensity is observed to increase due to presence of MZ particles. The methanol treated membranes exhibit considerable increase in permeability as the alcohol wash swells the membrane and opens up the free volume. Optimum performance is shown by methanol treated PIM-1/MZ MMM (10 wt%). We speculate that the permeation properties are adequately enhanced by MZ loading to PIM-1 matrix however at higher MZ loading, gas permeation properties are not further enhanced. This can be attributed to the poor filler-polymer adhesion and introduction of defects at higher filler concentration. Most favourable performance is exhibited by 10 wt% loading of MZ.

#### Acknowledgement

We would like to thank the Higher Education Commission of Pakistan for providing financial support under International Research Support Initiative Programme (IRSIP) for this research work to pursue at the University of Manchester, UK.

#### References

- W.F. Yong, F.Y. Li, Y.C. Xiao, T.S. Chung, Y.W. Tong, High performance PIM-1/Matrimid hollow fiber membranes for  $\text{CO}_2/\text{CH}_4$ ,  $\text{O}_2/\text{N}_2$  and  $\text{CO}_2/\text{N}_2$  separation, *J. Member. Sci.* 443 (2013) 156-169.
- M. Alberto, R. Bhavsar, J.M. Luque-Alled, A. Vijayaraghavan, P.M. Budd, P. Gorgojo, Impeded physical aging in PIM-1 membranes containing graphene-like fillers, *J. Member. Sci.* 563 (2018) 513-520.
- M. Lanč, K. Pilnáček, C.R. Mason, P.M. Budd, Y. Rogan, R. Malpass-Evans, O. Vopička, Gas sorption in polymers of intrinsic microporosity: The difference between solubility coefficients determined via time-lag and direct sorption experiments, *J. Member. Sci.* 570 (2019) 522-536.
- A. Alabi, L. Cseri, A. Al Hajaji, G. Szekely, P. Budd, L. Zou, Electrostatically-coupled graphene oxide nanocomposite cation exchange membrane, *J. Member. Sci.* 594 (2020) 117457.
- R.A. Kirk, M. Putintseva, A. Volkov, P.M. Budd, The potential of polymers of intrinsic microporosity (PIMs) and PIM/graphene composites for pervaporation membranes, *BMC. Chem. Eng.* 1 (2019) 18.
- Y. Liu, G. Liu, C. Zhang, W. Qiu, S. Yi, V. Chernikova, W. Koros, Enhanced  $\text{CO}_2/\text{CH}_4$  Separation Performance of a Mixed Matrix Membrane Based on Tailored MOF-Polymer Formulations, *Adv. Sci.* 5 (2018) 1800982.
- C.R. Mason, M.G. Buonomena, G. Golemme, P.M. Budd, F. Galiano, A. Figoli, V. Hnyek, New organophilic mixed matrix membranes derived from a polymer of intrinsic microporosity and silicalite-1, *Polym.* 54 (2013) 2222-2230.
- M. Khdhayyer, A.F. Bushell, P.M. Budd, M.P. Attfield, D. Jiang, A.D. Burrows, G. Clarizia, Mixed matrix membranes based on MIL-101 metal-organic frameworks in polymer of intrinsic microporosity PIM-1, *Sep. Purif. Technol.* 212 (2019) 545-554.
- A.Y. Alentiev, G.N. Bondarenko, Y.V. Kostina, V.P. Shantarovich, S.N. Klyamkin, V.P. Fedin, Y.P. Yampolskii, PIM-1/MIL-101 hybrid composite membrane material: Transport properties and free volume, *Petrol. Chem.* 54 (2014) 477-481.
- M.R. Khdhayyer, E. Esposito, A. Fuoco, M. Monteleone, L. Giorno, J.C. Jansen, P.M. Budd, Mixed matrix membranes based on UiO-66 MOFs in the polymer of intrinsic microporosity PIM-1, *Sep. Purif. Technol.* 173 (2017) 304-313.
- C. Ye, X. Wu, H. Wu, L. Yang, Y. Ren, Y. Wu, Z. Jiang, Incorporating nano-sized ZIF-67 to enhance selectivity of polymers of intrinsic microporosity membranes for biogas upgrading, *Chem. Engg. Sci.* 216 (2020) 115497.
- S. Sorribas, M. Tamaddondar, P.M. Budd, Membranes Made of Polymers of Intrinsic Microporosity (PIMs), *Comp. Member. Sci. Eng.* 216 (2017) 1-9.
- X.Y. Chen, H. Vinh-Thang, A.A. Ramirez, D. Rodrigue, S. Kaliaguine, Membrane gas separation technologies for biogas upgrading, *Rsc Adv.* 5 (2015) 24399-24448.
- M. Junaidi, C.P. Leo, A.L. Ahmad, S.N.M. Kamal, T.L. Chew, Carbon dioxide separation using asymmetric polysulfone mixed matrix membranes incorporated with SAPO-34 zeolite, *Fuel. Process. Technol.* 118 (2014) 125-132.
- C.I. Chaidou, G. Pantoleontos, D.E. Koutsonikolas, S.P. Kaldis, G.P. Sakellariopoulos, Gas separation properties of polyimide-zeolite mixed matrix membranes, *Sep. Sci. Technol.* 47 (2012) 950-962.
- A. Kausar, Membranes of polycarbonate/poly (styrene-co-allyl alcohol) reinforced with nano-zeolite-based filler for gas separation, *J. Chi. Adv. Mater. Sci.* 5 (2017) 33-46.
- Y. Li, L. Zhu, N. Grishkewich, K.C. Tam, J. Yuan, Z. Mao, X. Sui,  $\text{CO}_2$ -responsive cellulose nanofibers aerogels for switchable oil-water separation, *ACS Appl. Mater. Interfaces.* 11 (2019) 9367-9373.
- L.M. Robeson, The upper bound revisited, *J. Member. Sci.* 320 (2008) 390-400.
- K. Althumayri, W.J. Harrison, Y. Shin, J.M. Gardiner, C. Casiraghi, P.M. Budd, J.C. Jansen, The influence of few-layer graphene on the gas permeability of the high-free-volume polymer PIM-1, *Philos. Trans. R. Soc. A.* 374 (2016) 20150031.
- T. Mitra, R.S. Bhavsar, D.J. Adams, P.M. Budd, A.I. Cooper, PIM-1 mixed matrix membranes for gas separations using cost-effective hypercrosslinked nanoparticle fillers, *Chem. Comm.* 52 (2016) 5581-5584.
- A.F. Bushell, M.P. Attfield, C.R. Mason, P.M. Budd, Y. Yampolskii, L. Starannikova, M. Lanč, Gas permeation parameters of mixed matrix membranes based on the polymer of intrinsic microporosity PIM-1 and the zeolitic imidazolate framework ZIF-8, *J. Member. Sci.* 427 (2013) 48-62.
- P.M. Budd, N.B. McKeown, B.S. Ghanem, K.J. Msayib, D. Fritsch, L. Starannikova, V. Shantarovich, Gas permeation parameters and other physicochemical properties of a polymer of intrinsic microporosity: Polybenzodioxane PIM-1, *J. Member. Sci.* 325 (2008) 851-860.
- B. Satilmis, P.M. Budd, Base-catalysed hydrolysis of PIM-1: amide versus carboxylate formation, *Rsc Adv.* 4 (2014) 52189-52198.
- S.T. Muntha, M. Siddiq, A. Kausar, A. Khan, Mixed matrix membranes of polysulfone/polyimide reinforced with modified zeolite based filler: Preparation, properties and application, *Chinese J. Polym. Sci.* 36 (2018) 65-77.
- A.F. Bushell, M.P. Attfield, C.R. Mason, P.M. Budd, Y. Yampolskii, L. Starannikova, M. Lanč, Gas permeation parameters of mixed matrix membranes based on the polymer of intrinsic microporosity PIM-1 and the zeolitic imidazolate framework ZIF-8, *J. Member. Sci.* 427 (2013) 48-62.
- R.S. Bhavsar, T. Mitra, D.J. Adams, A.I. Cooper, P.M. Budd, Ultrahigh-permeance PIM-1 based thin film nanocomposite membranes on PAN supports for  $\text{CO}_2$  separation, *J. Member. Sci.* 564 (2018) 878-886.
- A. Fuoco, C. Rizzuto, E. Tocci, M. Monteleone, E. Esposito, P.M. Budd, J.C. Jansen, The origin of size-selective gas transport through polymers of intrinsic microporosity, *J. Mater. Chem A.* 7 (2019) 20121-20126.
- A.F. Bushell, P.M. Budd, M.P. Attfield, J.T. Jones, T. Hasell, A.I. Cooper, J.C. Jansen, Nanoporous organic polymer/cage composite membranes, *Angew. Chem. Int. Ed. Engl.* 52 (2013) 1253-1256.
- F.Y. Li, Y. Xiao, T.S. Chung, S. Kawi, High-performance thermally self-cross-linked polymer of intrinsic microporosity (PIM-1) membranes for energy development, *Macromolecules.* 45 (2012) 1427-1437.
- R. Chatti, A.K. Bansawal, J.A. Thote, V. Kumar, P. Jadhav, S.K. Lokhande, S.S. Rayalu, Amine loaded zeolites for carbon dioxide capture: Amine loading and adsorption studies, *Micropor. Mesopor. Matr.* 121 (2009) 84-89.
- Z. Tian, S. Wang, Y. Wang, X. Ma, K. Cao, D. Peng, Z. Jiang, Enhanced gas separation performance of mixed matrix membranes from graphitic carbon nitride nanosheets and polymers of intrinsic microporosity, *J. Member. Sci.* 514 (2016) 15-24.
- I. Borisov, D. Bakhtin, J.M. Luque-Alled, A. Rybakova, V. Makarova, A.B. Foster, E. Prestat, Synergistic enhancement of gas selectivity in thin film composite membranes of PIM-1, *J. Mater. Chem A.* 7 (2019) 6417-6430.
- H. Sanaeepur, R. Ahmadi, A.E. Amooghin, D. Ghanbari, A novel ternary mixed matrix membrane containing glycerol-modified poly (ether-block-amide)(Pebax 1657)/copper nanoparticles for  $\text{CO}_2$  separation, *J. Member. Sci.* 573 (2019) 234-246.
- A.F. Bushell, M.P. Attfield, C.R. Mason, P.M. Budd, Y. Yampolskii, L. Starannikova, M. Lanč, Gas permeation parameters of mixed matrix membranes based on the polymer of intrinsic microporosity PIM-1 and the zeolitic imidazolate framework ZIF-8, *J. Member. Sci.* 427 (2013) 48-62.
- M.L. Jue, C.S. McKay, B.A. McCool, M.G. Finn, R.P. Lively, Effect of Nonsolvent Treatments on the Microstructure of PIM-1, *Macromolecules.* 48 (2015) 5780-5790.
- Z. Wang, H. Ren, S. Zhang, F. Zhang, J. Jin, Polymers of intrinsic microporosity/metal-organic framework hybrid membranes with improved interfacial interaction for high-performance  $\text{CO}_2$  separation, *J. Mater. Chem A.* 5 (2017) 10968-10977.
- M. Alberto, R. Bhavsar, J.M. Luque-Alled, A. Vijayaraghavan, P.M. Budd, P. Gorgojo, Impeded physical aging in PIM-1 membranes containing graphene-like fillers, *J. Member. Sci.* 563 (2018) 513-520.
- B. Comesaña-Gándara, J. Chen, C.G. Bezzu, M. Carta, I. Rose, M.C. Ferrari, N.B. McKeown, Redefining the Robeson upper bounds for  $\text{CO}_2/\text{CH}_4$  and  $\text{CO}_2/\text{N}_2$  separations using a series of ultrapermeable benzotriptycene-based polymers of intrinsic microporosity, *Energy Environ. Sci.* 12 (2019) 2733-2740.